 doi:10.20944/preprints202212.0173.v1

Article

The Stable Operation Analysis of the DC Converter System into a Microgrid System, Taking into Account the Parameters of the Energy Source and the Own Parameters of the DC Converter

Denis Kotin [1] and Ilya Ivanov[2,*]

[1] Department of Electric Drive and Industry Automation, Novosibirsk State Technical University, 630073, Novosibirsk, Russia; d.kotin@corp.nstu.ru
[2] Department of Electric Drive and Industry Automation, Novosibirsk State Technical University, 630073, Novosibirsk, Russia; i.a.ivanov@corp.nstu.ru
* Correspondence: i.a.ivanov@corp.nstu.ru

Abstract: In this paper, the authors consider the influence of the type of power supply and the internal parameters of the DC-DC converter on the stability of the system at constant power load. The stability of the system under consideration is important in the design and development of the power supply system for an autonomous consumer. Such a typical system can be a DC microgrid. In the work, when analyzing the stability of the system, the power source is not considered an ideal voltage source, but the active-inductive nature of the voltage source is taken into account, which is equivalent to using a synchronous machine with permanent magnets. The Rauss-Hurwitz algebraic criterion was used as a criterion for analyzing the stability of the system. This will make it possible to build and analyze the areas and boundaries of the system's stability. As a result, the areas and boundaries of the stability of the system were presented. The general trend towards the behavior of the zone of instability of the system was given. At the same time, dependences describing the boundaries of instability are presented, which are combinations of parameters of the DC-DC converter, beyond which the system becomes unstable.It was found that the instability zone can begin with a combination of these parameters in the value of 81% of the power consumption, or from 20% of the DC-DC converter conversion factor, or the coefficient of proportionality of the input capacitance to the output equal to 1.The presented definitions of the instability limits can be used as a corrective device of the control system to ensure the stability of the system in the upper limits of the power consumption.

Keywords: DC Microgrid; DC-DC converter; stability analysis; stability boundary; CPL

1. Introduction

In modern energy industry, the concept of building an autonomous microgrid power supply system has become widespread. This is due to the transition to distributed energy and the use of the principle of distributed generation [1–4]. Systems built on the principle of microgrid are easier to transfer into synchronous mode with a common power supply system and it is possible to transfer it to an isolated mode [4–10]. Depending on the capacity of the intended consumer, the internal architecture of the microgrid varies. Two enlarged groups can be distinguished, these are microgrid with a common intermediate AC bus and microgrid with a common intermediate DC bus [2–4], [9].As a microgrid, it is necessary to consider not only power systems operating in parallel with the main power grid with a capacity of hundreds of kW, but also small-scale consumption facilities operating autonomously. Examples of low-energy objects operating outside the backbone network and corresponding to the principles of microgrids can be electric vehicles with the generation and consumption of electric energy on board, such as unmanned aerial

 doi:10.20944/preprints202212.0173.v1

vehicles, unmanned underwater vehicles, electric vehicles, etc., communication infrastructure objects, meteorological observation objects and much more. In these small energy consumption objects, the stability of the entire energy system is affected not only by the consumer like a load, but also by all the devices and converters included in this system. The stability energy system depends on the stable operation of the energy source. In this paper, the authors propose to consider the stability analysis of a microgrid autonomous object with a common intermediate DC bus, taking into account the type of energy source and the relationship between the parameters of the primary and secondary sides of a DC-DC converter with a load of the constant power load (CPL) type.

Analysis of the stability of the microgrid system is widespread, consider a number of works on this topic. In the work of Khaled Laib et al. [11] the stability of the DC microgrid system is considered. As an object under consideration, a mathematical description of the state space of the DC-DC converter and the dynamics of lines and buses is given. The authors analyze the impact on the stability of the parameters of the power transmission bus and the load for various layouts of the architecture of the microgrid system. In [12], the authors consider a DC microgrid system with a limited amount of power in the system, its consumption and accumulation. The work analyzes the operation of a system with idealized energy sources and a DC-DC converter of the standard form of writing in the form of a polynomial. Sarah Ansari et al. [13] in their work synthesize a robust algorithm for a DC-DC converter of a standard polynomial model. In [14], the authors consider the DC-microgrid system and the influence of various modifications of control algorithms on its operation. They consider a typical polynomial converter model and idealized energy sources. The authors of [15] consider the modes of charge and discharge in a DC microgrid. To analyze the system, a typical mathematical description of the DC-DC converter is used, and despite the fact that various modes of operation of energy storage devices are studied, they are considered idealized. In [16], the DC-DC converter is considered as a high-ranking polynomial model with an idealized energy source. In [17]the energy source has an active character, but the presence of nonlinearity is already taken into account due to the use of a single-diode solar panel replacement circuit. This effect is taken into account in the synthesis and analysis of the microgrid system. In the article[18]by authors Leony Ortiz et al., a general model of microgrid and analysis of energy flows in systems with high energy consumption is considered. Thus, the system considers the influence of various voltage sources on the overall condition of the network. But again, as in other works, the influence of the behavior of the energy source on the stability of the system is not taken into account, and the consumer is identified as the main cause of the instability of the system.

Summarizing not only the above works, but also [19]–[34], there is a general tendency to use a typical polynomial model that describes the relationship between the current of an inductive element and the voltage of the output capacitance of a DC-DC converter when working with an ideal voltage source. These simplifications of the system under consideration are explained by the fact that the implementation of a model that takes into account the dynamics of the energy source, the dynamics of the input circuit and the dynamics of the output circuit by the DC-DC converter is difficult due to the high degree of differential and non-linearity of the system used. In the proposed work, the authors decided to consider the impact on the stability of the operation of an active-inductive energy source and the relationship of the internal intrinsic parameters of the DC-DC converter. The proposed solution to the problem of the influence of the type of electrical energy sources on the stability of the entire system is achieved by evaluating the system according to the Routh-Hurwitz algebraic criterion. This estimate was obtained by combining the system parameters in the entire allowable range of system operation considered by the authors. Based on this, it is possible to form the boundary of possible combinations of system parameters, when passing through which the system becomes unstable. In this article, we present an algorithm for finding a given uncertainty boundary using the Routh-Hurwitz method.

Preprints (www.preprints.org) | NOT PEER-REVIEWED | Posted: 9 December 2022 doi:10.20944/preprints202212.0173.v1

2. Materials and Methods

To analyze the stable operation of the generating cell of a microgrid system with an intermediate DC bus, which includes equivalent circuits of a synchronous generator with an permanent magnets, presented as an EMF source with an active-inductive nature, a rectifier, DC / DC converter with input and output filters, we set a typical block diagram shown in Figure 1.

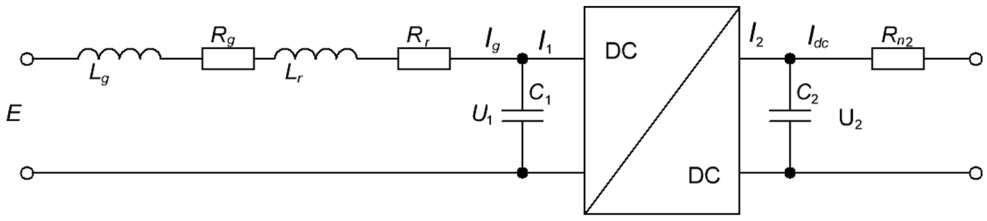

Figure 1. Block diagram.

The system consists of PMSM, rectifier, Bidirectional H-Bridge DC-DC converter input filter, , output filter, CPL[35], [36].To simplify the study of the presented system, there will be its effective values, since according to them, it will be possible, at their direction, to fully reason about the general purpose of the system.With this definition in mind, the mathematical description contains the structure:

$$\begin{cases} E = \left(R_g + R_r\right)I_g + \left(L_g + L_r\right)pI_g + U_1 = R_1 I_g + L_1 pI_g + U_1, \\ U_1 = \dfrac{1}{C_1 p}\left(I_g - I_1\right) \rightarrow I_g = C_1 pU_1 + I_1, \\ U_1 = \dfrac{U_1^2}{-P_n} I_1 = -R_{n1} I_1, \\ \dfrac{I_1}{I_2} = K, \\ U_2 = \dfrac{1}{C_2 p}\left(I_2 - I_{dc}\right) \rightarrow I_2 = C_2 pU_2 + I_{dc}, \\ U_2 = \dfrac{U_2^2}{P_n} I_{dc} = R_{n2} I_{dc}, \end{cases} \quad (1)$$

where E is the EMF, R_g, R_r, R_1 is the active component of the resistances of the generator, rectifier and the active resistance of the primary side of the DC-DC converter, L_g, L_r, L_1 is the inductive component of the resistances of the generator, rectifiers and the impedance inductive resistance of the primary side of the DC-DC converter, I_g - generator current, U_1, U_2 - voltage on the primary and secondary side of the DC-DC converter, I_1, I_2 - current in the primary and secondary part of the DC-DC converter, C_1, C_2 - capacitance of the input and output filters of the DC-DC converter, P_n - CPL, R_{n1}, R_{n2} - active component of the load resistance driven to the primaryand secondary side of the DC-DC converter.

According to the mathematical description presented above, the equivalent circuit will have the form shown in Figure 2.

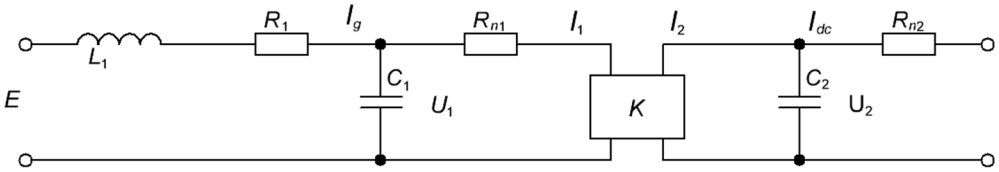

Figure 2. Equivalent circuit.

Preprints (www.preprints.org) | NOT PEER-REVIEWED | Posted: 9 December 2022 doi:10.20944/preprints202212.0173.v1

To simplify the analysis, namely the influence of the load on the stability of the system, we bring the parameters of the secondary side to the primary side:

$$\frac{U_2}{U_1} = K \rightarrow U_2 = KU_1, \tag{2}$$

$$R_{n2} = \frac{U_2^2}{P_n} = \frac{(KU_1)^2}{P_n} = K^2 \frac{U_1^2}{P_n} = K^2 R_{n1}, \tag{3}$$

$$C_2 = aC_1, \tag{4}$$

where a is a coefficient describing the ratio of input and output DC/DC converter.

For analysis from system (1) and taking into account the accepted parameters (2)-(4), a small signal model:

$$p\begin{bmatrix} i_{\Delta g} \\ i_{\Delta 1} \\ i_{\Delta dc} \end{bmatrix} = \begin{bmatrix} -\frac{R_1}{L_1} & \frac{R_{n1}}{L_1} & 0 \\ -\frac{1}{C_1 R_{n1}} & \frac{1}{C_1 R_{n1}} & 0 \\ 0 & \frac{1}{K^3 a C_1 R_{n1}} & -\frac{1}{K^2 a C_1 R_{n1}} \end{bmatrix} \times \begin{bmatrix} i_{\Delta g} \\ i_{\Delta 1} \\ i_{\Delta dc} \end{bmatrix} + \begin{bmatrix} \frac{1}{L_1} \\ 0 \\ 0 \end{bmatrix} \times \begin{bmatrix} E_\Delta \\ 0 \\ 0 \end{bmatrix}, \tag{5}$$

To determine the stable performance of the system, a general transfer function of the entire system is characteristic (6).

General transfer function:

$$W_g(s) = \frac{i_{\Delta dc}(s)}{E_\Delta(s)} = \frac{1}{T_3 s^3 + T_2 s^2 + T_1 s + T_0}, \tag{6}$$

where:

$$T_3 = -aL_1 C_1 C_2 K^3 R_{n1}^2, \tag{7}$$

$$T_2 = aK^3 C_1 R_{n1} L_1 - aK^3 C_1^2 R_1 R_{n1}^2 - KL_1 C_1 R_{n1}, \tag{8}$$

$$T_1 = KL_1 - KC_1 R_1 R_{n1} + aK^3 R_1 C_1 R_{n1} - aK^3 C_2 R_{n1}^2, \tag{9}$$

$$T_0 = K(R_1 - R_{n1}), \tag{10}$$

For further analysis, we compose the equation of the first determinanta_0 of the Routh-Hurwitz matrix:

$$a_0 = T_2 T_1 - T_0 T_3 = f(a, K, R_{n1}) > 0 \tag{11}$$

$$\begin{aligned} f(a, K, R_{n1}) = \\ = C_1^2 R_1 (a^2 K^6 R_{n1}^4) + C_1^3 R_1^2 (aK^4 R_{n1}^3) - C_1^3 R_1^2 (a^2 K^6 R_{n1}^3) - C_1^2 L_1 (a^2 K^6 R_{n1}^3) + \\ + C_1^2 (a^2 K^4 R_{n1}^3) - C_1^2 L_1 (aK^4 R_n^3) + C_1 L_1^2 (aK^4 R_{n1}^2) - C_1^2 L_1 R_1 (aK^4 R_{n1}^2) - \\ - C_1^2 L_1 R_1 (aK^4 R_{n1}^2) + C_1^2 L_1 R_1 (K^2 R_{n1}^2) + C_1^2 L_1 R_1 (aK^6 R_{n1}^2) - \\ - C_1^2 L_1 R_1 (aK^4 R_{n1}^2) + C_1^2 L_1 R_1 (aK^4 R_{n1}^2) - C_1 L_1^2 (K^2 R_{n1}). \end{aligned} \tag{12}$$

Since the analysis and construction of a four-dimensional space is difficult, we will analyze its three-dimensional projections on each of the axes. Also, to simplify the analysis of three-dimensional figures, which are projections of a four-dimensional space, we will divide them into a set of surfaces. Thus, we can say that in order to evaluate the nature of the behavior of a four-dimensional spacer, it will be necessary to project it onto three three-dimensional spaces, and then the resulting three-dimensional figures, which will be divided into the n-th number of surfaces:

Preprints (www.preprints.org) | NOT PEER-REVIEWED | Posted: 9 December 2022 doi:10.20944/preprints202212.0173.v1

$$a_0 = f(a, K, R_{n1}) = \begin{cases} a_0 = f\big(K(a), R_{n1}(a)\big) \\ a_0 = f\big(a(K), R_{n1}(K)\big) \\ a_0 = f\big(a(R_{n1}), K(R_{n1})\big) \end{cases}. \quad (13)$$

To determine the exact boundary of the stability of the system, it was solved to find the curves describing the intersections of the surfaces of zeros with the corresponding surfaces:

$$a_0 = f(a, K, R_{n1}) = 0 = \\ = \begin{cases} a_0 = f\big(K(a), R_{n1}(a)\big) = 0 \\ a_0 = f\big(a(K), R_{n1}(K)\big) = 0 \\ a_0 = f\big(a(R_{n1}), K(R_{n1})\big) = 0 \end{cases} = \begin{cases} a_0 = f_{a=\mathrm{var}}(K) = 0 \\ a_0 = f_{a=\mathrm{var}}(R_{n1}) = 0 \\ a_0 = f_{K=\mathrm{var}}(a) = 0 \\ a_0 = f_{K=\mathrm{var}}(R_{n1}) = 0' \\ a_0 = f_{R_{n1}=\mathrm{var}}(a) = 0 \\ a_0 = f_{R_{n1}=\mathrm{var}}(K) = 0 \end{cases} \quad (14)$$

i.e., we obtain a function of the curve describing the intersection of two surfaces for different values of the constant coefficient with the zero plane.

The system of equations (13) represents the functions of projections onto the three-dimensional surface of the four-dimensional space a_0 onto each space corresponding to one of the excluded variables. And the system of equation (14) describes the intersection curves of the obtained surfaces (13) with the zero plane of the system. The resulting curves (14) represent nothing more than a combination of parameters into systems for which the system is unstable.

To determine the functions of these surfaces, we interpolate in the region of the boundary of the intersection of the surfaces of the systems.

3. Results

To implement this, we will set a discrete step for changing the constant parameters and variable parameters of the function. In the first case, the change in the coefficient of dependence of the output capacitance on the input a, a constant parameter. It will be in the range from 1 to 10 with a step of 1, and the variable coefficients of the function, transformation ratio$K$ from 0.5 to 3. The equivalent active resistance of the power consumption R_{n1} in the range of recalculation of the power consumption from 1 kW to 75 kW.

In the second case, the change in the transformation ratio K, a constant parameter. It will be in the range from 0.5 to 3 in increments of 0.5, and the variable coefficients of the function, the coefficient of dependence of the output capacitance on the input a from 1 to 10.The equivalent active resistance of the consumed power R_{n1} in the range of recalculation of power consumption from 1 kW to 75 kW.

In the third case, the change in the equivalent active resistance of the power consumption R_{n1}, a constant parameter.It will be in the CPL range from 1 kW to 75 kW in increments of 5 kW, and the variable coefficients of the function. The dependence coefficient of the output capacitance on the input a from 1 to 10, and the transformation ratio K is from 0.5 to 3.

Figures 3 - 8 show the surfaces for two extreme values of the constant parameter when using the system of equations (13).

Preprints (www.preprints.org) | NOT PEER-REVIEWED | Posted: 9 December 2022 doi:10.20944/preprints202212.0173.v1

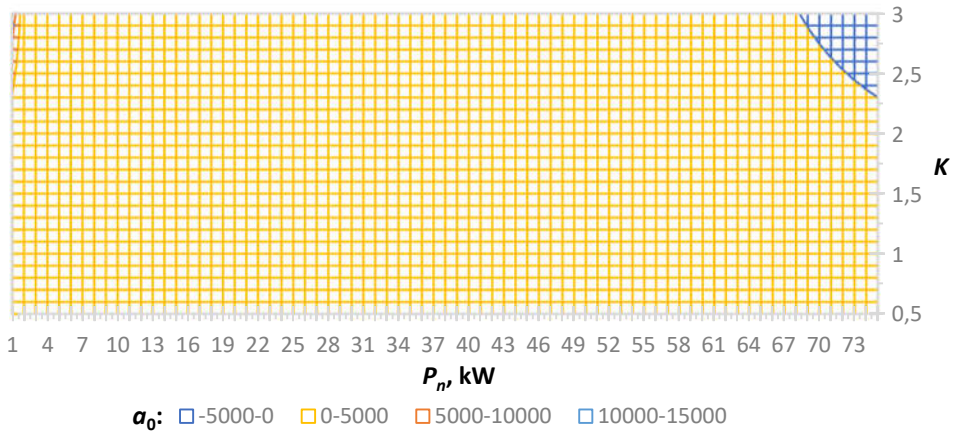

Figure 3. Surface $a_0=f(K, P_n)$, for $a = 1$.

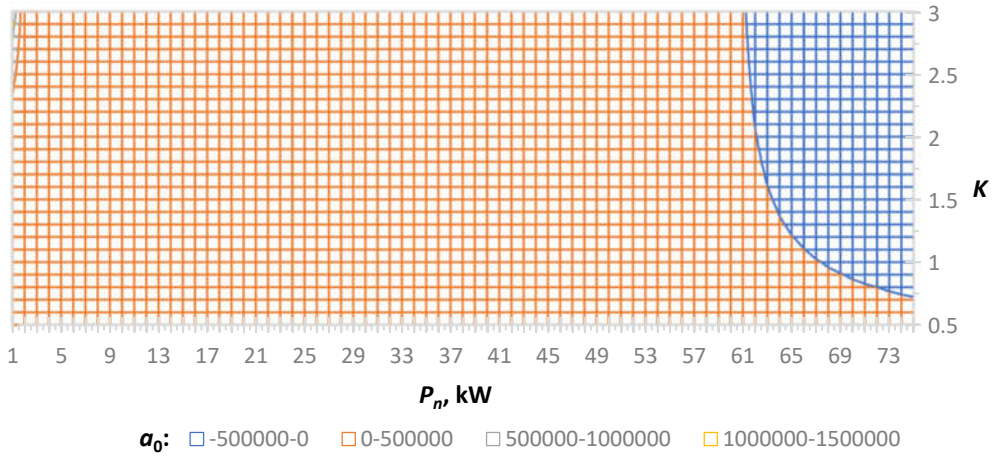

Figure4. Surface $a_0=f(K, P_n)$, for $a = 10$.

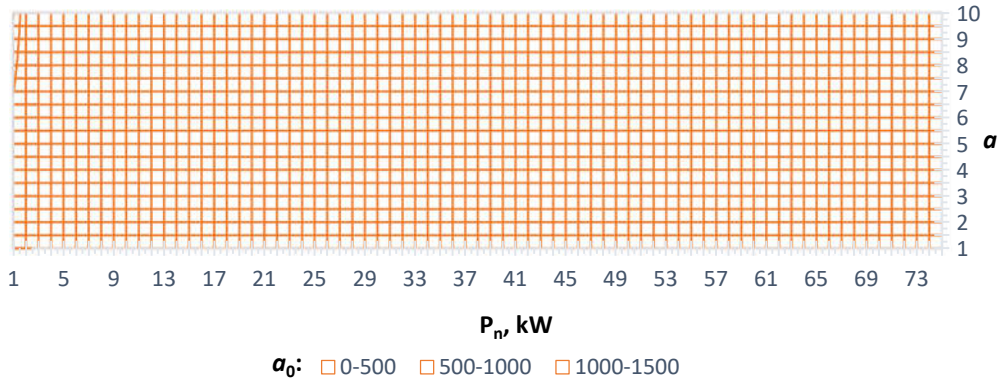

Figure5. Surface $a_0=f(a, P_n)$, for $K = 0.5$.

Preprints (www.preprints.org) | NOT PEER-REVIEWED | Posted: 9 December 2022 doi:10.20944/preprints202212.0173.v1

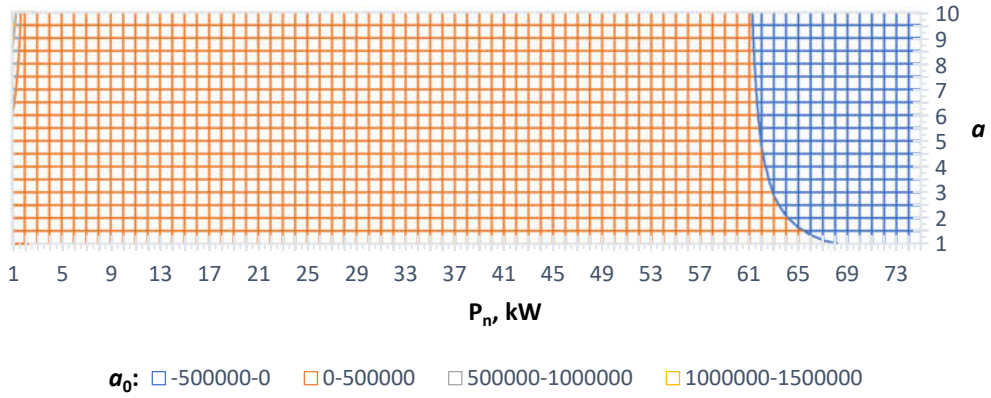

Figure6. Surface a_0=f(a, P_n), for$K$ = 3.

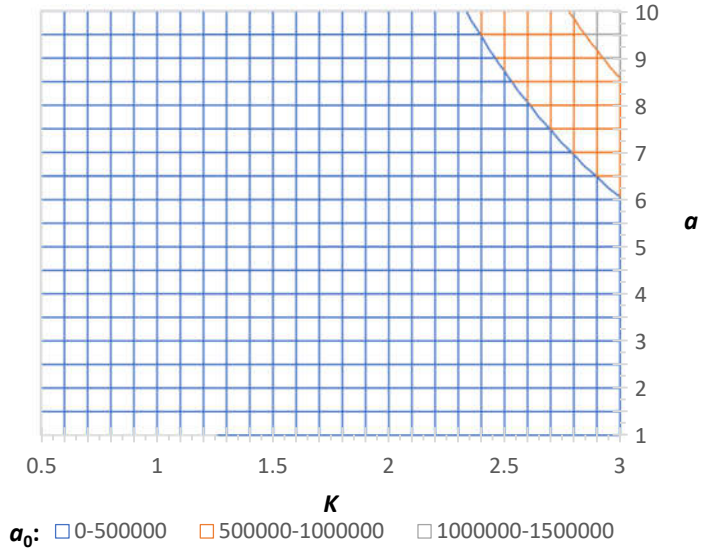

Figure7. Surface a_0=f(a, K), forP_n = 1 kW.

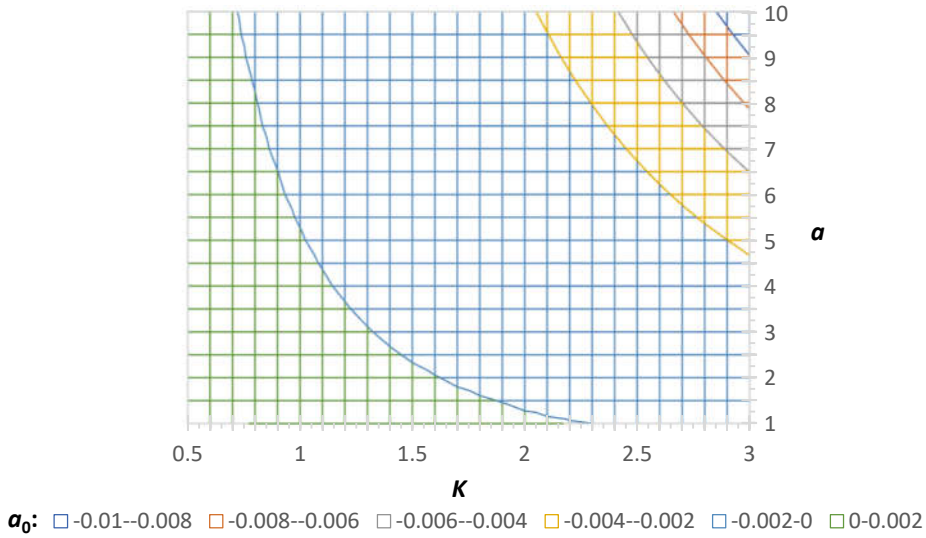

Figure8. Surface a_0=f(a, K), forP_n = 75 kW.

Preprints (www.preprints.org) | NOT PEER-REVIEWED | Posted: 9 December 2022 doi:10.20944/preprints202212.0173.v1

In all three sets of surfaces, a system instability zone appears, and when any constant surface parameter changes, this zone changes, namely, the system instability zone increases.

After obtaining the interpolated values, we construct curves that describe the stability boundary of the system for different values of the coefficients of proportionality of the output capacitance to the input capacitance with a change in the load and transfer coefficient, a set of curves is shown in Figures 9–14.

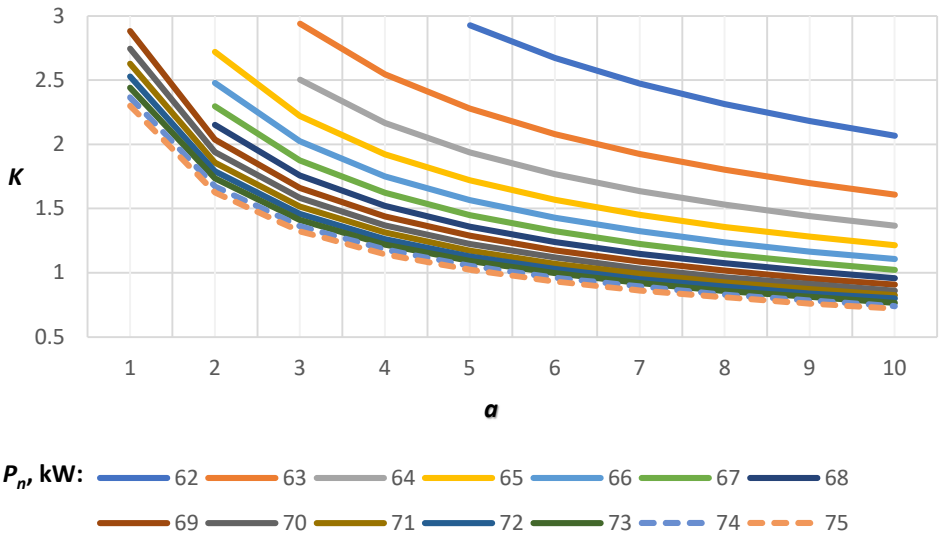

Figure 9. System stability limit's function $a_0=f_{a=var}(K)$, for P_n = const.

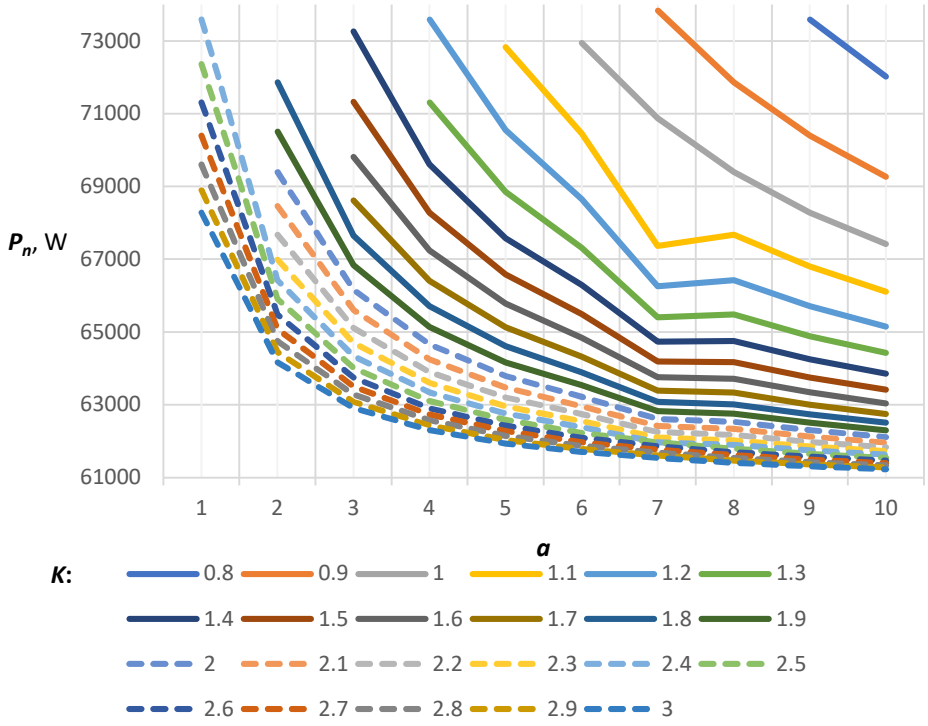

Figure10. System stability limit`s function $a_0=f_{a=var}(P)$, for K = const.

Preprints (www.preprints.org) | NOT PEER-REVIEWED | Posted: 9 December 2022 doi:10.20944/preprints202212.0173.v1

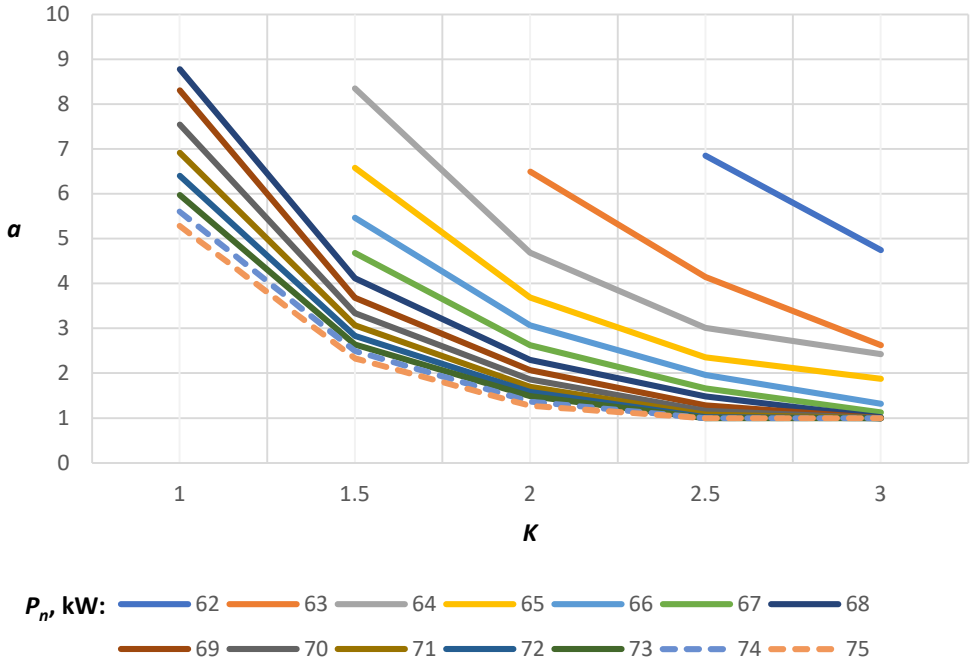

Figure11. System stability limit`s function$a_0=f_{K=var}(A)$, forP_n = const.

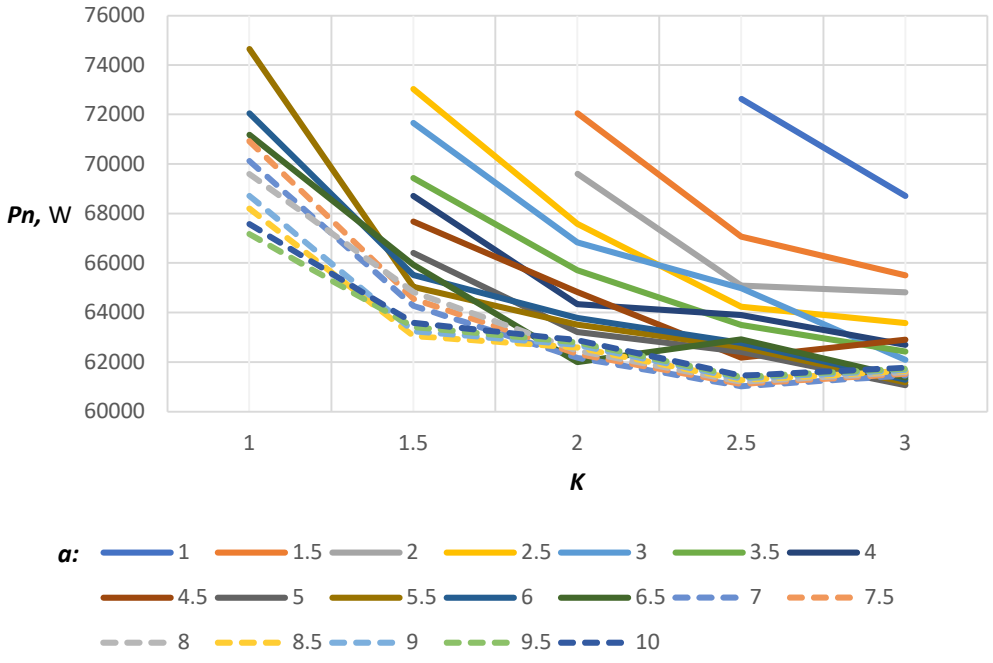

Figure12. System stability limit`s function$a_0=f_{K=var}(P)$, for$a$ = const.

Preprints (www.preprints.org) | NOT PEER-REVIEWED | Posted: 9 December 2022 doi:10.20944/preprints202212.0173.v1

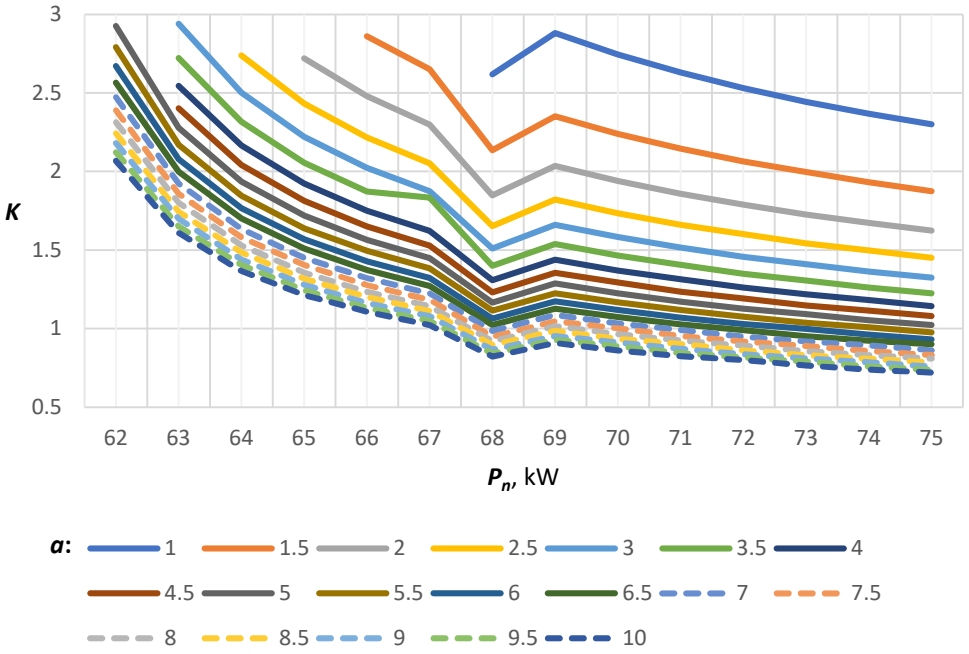

Figure13. System stability limit`s function$a_0=f_{P=var}(K)$, for$a$ = const.

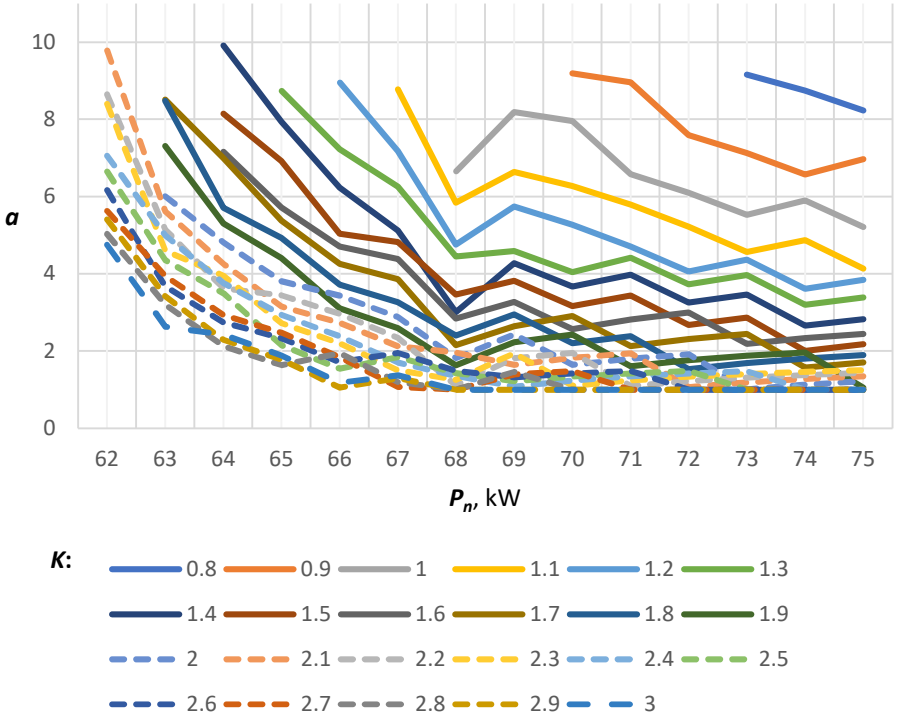

Figure14. System stability limit`s function$a_0=f_{P=var}(a)$, for$K$ = const.

Let's analyze figures 9 - 14 to determine the patterns of behavior of the system's stability boundary. The figures describing the behavior of the resistance stability boundary under the condition P = const, the functions $a_0=f_{a=var}(K)$, fig. 9, and $a_0=f_{K=var}(A)$, fig. 11, it can be seen that with an increase in the power consumption, the instability boundary expands

Preprints (www.preprints.org) | NOT PEER-REVIEWED | Posted: 9 December 2022 doi:10.20944/preprints202212.0173.v1

both in terms of the gain parameter and in terms of the capacitance proportionality factor. The same behavior of the stability boundary can be traced under the condition a = const, functions $a_0=f_{K=var}(P)$, fig. 12, and $a_0=f_{P=var}(K)$, fig. 13, and under the condition K = const, the functions $a_0=f_{a=var}(P)$, fig. 10, and $a_0=f_{P=var}(a)$, fig. 14.

4. Discussion

The results obtained demonstrate that an instability zone appears in the DC-DC converter system. The region of the instability zone is affected by three indicators that connect the primary and secondary sides of the DC-DC converters. Since, as a result of the analysis, 6 sets of curves were obtained that describe the movement of the stability boundary, it is necessary to determine the most convenient class of curves for the synthesis of the control system. According to the authors, the most convenient for the synthesis of the control system will be the curves given by the condition a = const, such sets of curves are the functions $a_0= f_{K=var}(P)$, figure 12, and $a_0= f_{P=var}(K)$, figure 13. Use as the reference parameter of the coefficient a is explained by the fact that this coefficient has a constant value and is set at the stage of system development. From figure 12 it can be seen that from the coefficient of proportionality of the capacitance in the system, distortions arise in the monotonicity of the decrease in the functions of the stability boundaries of the system. At a = 4.5, an extremum appears in the system at a value of K = 2.5. At a = 6.5, two inflections of the function appear in the system at K = 2 and K = 2.5. And within the boundaries of a from 7 to 10, an extremum is observed in the system at the point K = 2.5. Figure 13 shows that the class of functions has an identical form of monotonicity over its entire range of definition. A point stands out from the general form of monotony at a power of 68 kW. At this point, there is a local minimum of the function, and at the point of 69 kW there is an inflection point for all functions. Moreover, it should be noted that with an increase in the coefficient, a, there is a decrease in the value of the maximum deviation of the gain at the point of 68 kW, relative to the general nature of the decrease in the function.

As can be seen from the description of the behavior of the class of functions of the stability boundary of the system, the simplest in terms of the formation of a generalized mathematical function of the upper boundary of the power factor is the class of curves shown in Figure 13. Based on this description, it is possible to develop a nonlinear controller of the function of the form $K= f(P_{n})$, for known fixed a. This controller will limit the energy transfer coefficient K between the primary and secondary side of the DC-DC converter to ensure a stable mode of operation of the system.

The study of the influence of this additional controller on the control system will be carried out in the next work of the team of authors. An analysis of the structure of the control system with its use will also be carried out. This will make it possible to perform structural optimization of the system control algorithm.

5. Conclusions

In the work done, the authors analyzed the stability of the DC-DC converter system of the H-bridge type using an active-inductive energy source in the form of a synchronous generator with permanent magnets as a power source under a load of the CPL type. A mathematical model was obtained in the form of a small signal. This model links the parameters of the primary and secondary side of the DC-DC converter. The authors establish a mathematical relationship between these parameters and form a group of parameters responsible for the stability of the system. These parameters are the power transfer coefficient between the secondary and primary side (K), the equivalent active resistance for CPL (R_{n1}), and the proportionality factor between the input and output filter capacitance (a). Using this group of parameters and the Routh-Hurwitz stability criterion, a function of three variables $f(a, K, P)$ was formulated. Based on the analysis of this function, a collection of parameter planes and a class of functions of the stability boundaries of the system were obtained. When analyzing the set of curves of the stability boundaries, a general tendency towards the behavior of functions was formulated, namely, a monotonous

decrease in the function with a run on the main parameter under consideration. Based on this, we can say that there is an increase in the surface area in which the system is unstable. To solve this problem, the authors substantiated the choice of the most convenient set of curves for the system stability boundaries and described in more detail the dynamics of their behavior. These curves are the curves of the functions $a_0=f_{K=var}(P)$ and $a_0=f_{P=var}(K)$, since one of the variables in them is a design constant and in rare cases changes during the operation of the system. Such parameters are the coefficient of proportionality between the capacitance of the input and output filters (a).The use of the dependencies obtained indicates that the use of classical controllers will be difficult, since it is necessary to organize the operation of the system according to the function of two variables and at the same time introduce nonlinear control systems for elements. Therefore, the authors consider it expedient to switch to intelligent control systems. The use of such systems with the application of the considered restrictions to ensure the stable operation of the system will be considered in the following works of the team of authors.

Author Contributions: For research articles with several authors, a short paragraph specifying their individual contributions must be provided. The following statements should be used "Conceptualization, X.X. and Y.Y.; methodology, X.X.; software, X.X.; validation, X.X., Y.Y. and Z.Z.; formal analysis, X.X.; investigation, X.X.; resources, X.X.; data curation, X.X.; writing—original draft preparation, X.X.; writing—review and editing, X.X.; visualization, X.X.; supervision, X.X.; project administration, X.X.; funding acquisition, Y.Y. All authors have read and agreed to the published version of the manuscript."Please turn to the CRediT taxonomyfor the term explanation. Authorship must be limited to those who have contributed substantially to the work reported.

Funding: Please add: "This research received no external funding" or "This research was funded by NAME OF FUNDER, grant number XXX" and "The APC was funded by XXX". Check carefully that the details given are accurate and use the standard spelling of funding agency names at https://search.crossref.org/funding. Any errors may affect your future funding.

Data Availability Statement: In this section, please provide details regarding where data supporting reported results can be found, including links to publicly archived datasets analyzed or generated during the study. Please refer to suggested Data Availability Statements in section "MDPI Research Data Policies" at https://www.mdpi.com/ethics. If the study did not report any data, you might add "Not applicable" here.

Acknowledgments: In this section, you can acknowledge any support given which is not covered by the author contribution or funding sections. This may include administrative and technical support, or donations in kind (e.g., materials used for experiments).

Conflicts of Interest: Declare conflicts of interest or state "The authors declare no conflict of interest." Authors must identify and declare any personal circumstances or interest that may be perceived as inappropriately influencing the representation or interpretation of reported research results. Any role of the funders in the design of the study; in the collection, analyses or interpretation of data; in the writing of the manuscript; or in the decision to publish the results must be declared in this section. If there is no role, please state "The funders had no role in the design of the study; in the collection, analyses, or interpretation of data; in the writing of the manuscript; or in the decision to publish the results".

Nomenclature

The symbols used in this paper are defined below.

Indices and Numbers	
g	generator parameters
r	rectifier parameters
n	laod parameters
dc	DC bus parameters
1	primary side parameters
2	secondary side parameters

Preprints (www.preprints.org) | NOT PEER-REVIEWED | Posted: 9 December 2022 doi:10.20944/preprints202212.0173.v1

Variables	
E	EMF
U	voltage
I	current
R	active component of the resistances
L	inductive component of the resistances
C	capacitance of filters
a	coefficient of proportionality between the capacitance of the input and output filters
K	transformation ratio
a_0	first determinant of the Routh-Hurwitz matrix
P	constant power load

References

1. D. E. Olivares *et al.*, "Trends in microgrid control," *IEEE Trans Smart Grid*, vol. 5, no. 4, pp. 1905–1919, 2014, doi: 10.1109/TSG.2013.2295514.
2. A. El-Shahat and S. Sumaiya, "DC-Microgrid System Design, Control, and Analysis," *Electronics 2019, Vol. 8, Page 124*, vol. 8, no. 2, p. 124, Jan. 2019, doi: 10.3390/ELECTRONICS8020124.
3. M. Rezkallah, A. Chandra, B. Singh, and S. Singh, "Microgrid: Configurations, control and applications," *IEEE Trans Smart Grid*, vol. 10, no. 2, pp. 1290–1302, Mar. 2019, doi: 10.1109/TSG.2017.2762349.
4. S. Sen and V. Kumar, "Microgrid control: A comprehensive survey," *Annu Rev Control*, vol. 45, pp. 118–151, Jan. 2018, doi: 10.1016/J.ARCONTROL.2018.04.012.
5. I. Khan, Y. Xu, H. Sun, and V. Bhattacharjee, "Distributed Optimal Reactive Power Control of Power Systems," *IEEE Access*, vol. 6, pp. 7100–7111, Dec. 2017, doi: 10.1109/ACCESS.2017.2779806.
6. C. Wan, M. Huang, C. K. Tse, and X. Ruan, "Stability of interacting grid-connected power converters," *Journal of Modern Power Systems and Clean Energy*, vol. 1, no. 3, pp. 249–257, Jan. 2013, doi: 10.1007/S40565-013-0034-Y/TABLES/6.
7. Y. Gui, F. Blaabjerg, X. Wang, J. D. Bendtsen, D. Yang, and J. Stoustrup, "Improved DC-Link Voltage Regulation Strategy for Grid-Connected Converters," *IEEE Transactions on Industrial Electronics*, vol. 68, no. 6, pp. 4977–4987, Jun. 2021, doi: 10.1109/TIE.2020.2989720.
8. Y. v. Pavan Kumar and R. Bhimasingu, "Renewable energy based microgrid system sizing and energy management for green buildings," *Journal of Modern Power Systems and Clean Energy*, vol. 3, no. 1, pp. 1–13, Jan. 2015, doi: 10.1007/S40565-015-0101-7/FIGURES/26.
9. A. Alfergani, A. Khalil, and Z. Rajab, "Networked control of AC microgrid," *Sustain Cities Soc*, vol. 37, pp. 371–387, Feb. 2018, doi: 10.1016/J.SCS.2017.11.010.
10. P. O. Kriett and M. Salani, "Optimal control of a residential microgrid," *Energy*, vol. 42, no. 1, pp. 321–330, Jun. 2012, doi: 10.1016/J.ENERGY.2012.03.049.
11. K. Laib, J. Watson, Y. Ojo, and I. Lestas, "Decentralized Stability Conditions in DC Microgrids," *Proceedings of the IEEE Conference on Decision and Control*, vol. 2021-December, pp. 5659–5664, 2021, doi: 10.1109/CDC45484.2021.9683386.
12. B. E. Noriega, R. T. Pinto, and P. Bauer, "Sustainable DC-microgrid control system for electric-vehicle charging stations," *2013 15th European Conference on Power Electronics and Applications, EPE 2013*, 2013, doi: 10.1109/EPE.2013.6634620.
13. S. Ansari, J. Zhang, and K. Iqbal, "Modeling, stability analysis and simulation of buck converter in a DC microgrid," *2021 IEEE Kansas Power and Energy Conference, KPEC 2021*, 2021, doi: 10.1109/KPEC51835.2021.9446255.
14. P. S. N. Filho, J. P. C. Silveira, P. J. D. S. Neto, M. V. de Paula, T. A. D. S. Barros, and E. R. Filho, "Modeling and Experimental Evaluation of Energy Storage Emulator for Microgrids Application," *IEEE J EmergSel Top Power Electron*, vol. 9, no. 6, pp. 6662–6670, Dec. 2021, doi: 10.1109/JESTPE.2021.3055079.
15. S. Punna, R. Mailugundla, and S. R. Salkuti, "Design, Analysis and Implementation of Bidirectional DC-DC Converters for HESS in DC Microgrid Applications," *Smart Cities 2022, Vol. 5, Pages 433-454*, vol. 5, no. 2, pp. 433–454, Mar. 2022, doi: 10.3390/SMARTCITIES5020024.
16. N. Ghanbari, P. M. Shabestari, A. Mehrizi-Sani, and S. Bhattacharya, "State-space modeling and reachability analysis for a DC microgrid," *Conference Proceedings - IEEE Applied Power Electronics Conference and Exposition - APEC*, vol. 2019-March, pp. 2882–2886, May 2019, doi: 10.1109/APEC.2019.8721914.
17. E. Lodhi *et al.*, "A Dragonfly Optimization Algorithm for Extracting Maximum Power of Grid-Interfaced PV Systems," *Sustainability 2021, Vol. 13, Page 10778*, vol. 13, no. 19, p. 10778, Sep. 2021, doi: 10.3390/SU131910778.
18. L. Ortiz, R. Orizondo, A. Águila, J. W. González, G. J. López, and I. Isaac, "Hybrid AC/DC microgrid test system simulation: grid-connected mode," *Heliyon*, vol. 5, no. 12, p. e02862, Dec. 2019, doi: 10.1016/J.HELIYON.2019.E02862.
19. T. John and S. P. Lam, "Voltage and frequency control during microgrid islanding in a multi-area multi-microgrid system," *IET Generation, Transmission & Distribution*, vol. 11, no. 6, pp. 1502–1512, Apr. 2017, doi: 10.1049/IET-GTD.2016.1113.
20. F. Chavira, S. Ortega-Cisneros, and J. Rivera, "A Novel Sliding Mode Control Scheme for a PMSG-Based Variable Speed Wind Energy Conversion System," *Energies 2017, Vol. 10, Page 1476*, vol. 10, no. 10, p. 1476, Sep. 2017, doi: 10.3390/EN10101476.
21. V. T. Minh and A. A. Rashid, "Modeling and model predictive control for hybrid electric vehicles," *International Journal of Automotive Technology*, vol. 13, no. 3, pp. 477–485, Apr. 2012, doi: 10.1007/S12239-012-0045-0.
22. Y. Li, Y. Peng, and X. Wang, "Seamless switching power sharing control method in a hybrid DC-AC microgrid by the isolated two-stage converter based on SST," *IET Power Electronics*, vol. 14, no. 7, pp. 1384–1396, May 2021, doi: 10.1049/PEL2.12135.
23. M. A. M. Ramli, H. R. E. H. Bouchekara, and A. S. Alghamdi, "Optimal sizing of PV/wind/diesel hybrid microgrid system using multi-objective self-adaptive differential evolution algorithm," *Renew Energy*, vol. 121, pp. 400–411, Jun. 2018, doi: 10.1016/J.RENENE.2018.01.058.

24. M. A. Hossain, H. R. Pota, M. J. Hossain, and A. M. O. Haruni, "Active power management in a low-voltage islanded microgrid," *International Journal of Electrical Power & Energy Systems*, vol. 98, pp. 36–47, Jun. 2018, doi: 10.1016/J.IJEPES.2017.11.019.
25. A. Chadha and M. K. Kazimierczuk, "Small-Signal Modeling of Open-Loop PWM Tapped-Inductor Buck DC-DC Converter in CCM," *IEEE Transactions on Industrial Electronics*, vol. 68, no. 7, pp. 5765–5775, Jul. 2021, doi: 10.1109/TIE.2020.2996157.
26. S. Kapat, G. R. Chilukuri, and S. Jash, "Small-Signal Modeling of SIMO DC-DC Converters and Comparative Continuous/Discrete-Time Results," *2020 IEEE 21st Workshop on Control and Modeling for Power Electronics, COMPEL 2020*, Nov. 2020, doi: 10.1109/COMPEL49091.2020.9265749.
27. A. Elserougi, I. Abdelsalam, A. Massoud, and S. Ahmed, "A Non-Isolated Hybrid-Modular DC-DC Converter for DC Grids: Small-Signal Modeling and Control," *IEEE Access*, vol. 7, pp. 132459–132471, 2019, doi: 10.1109/ACCESS.2019.2941249.
28. E. Ugur and B. Vural, "Comparison of different small signal modeling methods for bidirectional DC-DC converter," *3rd International Conference on Renewable Energy Research and Applications, ICRERA 2014*, pp. 913–915, Jan. 2014, doi: 10.1109/ICRERA.2014.7016518.
29. R. Han, J. M. Guerrero, M. Tucci, A. Martinelli, and G. Ferrari-Trecate, "Plug-and-Play Voltage/Current Stabilization DC Microgrid Clusters with Grid-Forming/Feeding Converters," *Proceedings of the American Control Conference*, vol. 2018-June, pp. 5362–5367, Aug. 2018, doi: 10.23919/ACC.2018.8430783.
30. V. M. Iyer*et al.*, "An Active Voltage Stabilizer for a DC Microgrid System," *IEEE Access*, vol. 9, pp. 86786–86800, 2021, doi: 10.1109/ACCESS.2021.3087543.
31. M. Pourmohammad, M. Toulabi, M. Rayati, and S. A. Khajehoddin, "Load type impacts on the stability and robustness of DC microgrids," *International Journal of Electrical Power & Energy Systems*, vol. 140, p. 108036, Sep. 2022, doi: 10.1016/J.IJEPES.2022.108036.
32. Z. Zhang *et al.*, "Large-signal stability analysis of islanded DC microgrids with multiple types of loads," *International Journal of Electrical Power & Energy Systems*, vol. 143, p. 108450, Dec. 2022, doi: 10.1016/J.IJEPES.2022.108450.
33. X. Jin, Y. Shen, and Q. Zhou, "A systematic review of robust control strategies in DC microgrids," *The Electricity Journal*, vol. 35, no. 5, p. 107125, Jun. 2022, doi: 10.1016/J.TEJ.2022.107125.
34. H. Liu *et al.*, "Small-signal Analysis of DC Microgrid and Multi-objective Optimization Segmented Droop Control Suitable for Economic Dispatch," *Journal of Modern Power Systems and Clean Energy*, vol. 8, no. 3, pp. 564–572, May 2020, doi: 10.35833/MPCE.2018.000878.
35. V. v. Vdovin, D. P. Visloguzov, V. A. Klan, D. A. Kotin, and A. v. Smetannikov, "DC mains backup power system for frequency-controlled electric drive," *International Conference of Young Specialists on Micro/Nanotechnologies and Electron Devices, EDM*, pp. 387–391, 2014, doi: 10.1109/EDM.2014.6882554.
36. S. Inoue and H. Akagi, "A bidirectional DC-DC converter for an energy storage system with galvanic isolation," *IEEE Trans Power Electron*, vol. 22, no. 6, pp. 2299–2306, Nov. 2007, doi: 10.1109/TPEL.2007.909248.